Global and Planetary Change 205 (2021) 103589

Contents lists available at ScienceDirect

Global and Planetary Change

journal homepage: www.elsevier.com/locate/gloplacha

A 350-year multiproxy record of climate-driven environmental shifts in the Amundsen Sea Polynya, Antarctica

So-Young Kim [a,*], Dhongil Lim [b], Lorena Rebolledo [c], Taewook Park [a,*], Oliver Esper [d], Práxedes Muñoz [e], Hyoung Sul La [a], Tae Wan Kim [a], SangHoon Lee [a]

[a] Division of Ocean Sciences, Korea Polar Research Institute, Incheon 21990, Republic of Korea
[b] South Sea Research Institute, Korea Institute of Ocean Science & Technology, Geoje 53201, Republic of Korea
[c] Instituto Antártico Chileno (INACH), Plaza Muñoz Gamero 1055, Punta Arenas, Chile, Centro Fondap-Ideal, Punta Arenas, Chile
[d] Alfred Wegener Institute, Helmholtz Centre for Polar and Marine Research, Bremerhaven, Germany
[e] Departamento de Biología Marina, Universidad Católica del Norte, Larrondo 1281, Coquimbo, Chile

ARTICLE INFO

Keywords:
Amundsen Sea Polynya
Sediment
Circumpolar Deep Water
Atmospheric circulation

ABSTRACT

With a growing concern over rapid Antarctic ice loss in recent years, the Amundsen Sea, one of the fastest-melting areas in Antarctica, currently becomes a hotspot for the Earth sciences in the context of its linkage to global climate. As a center of strong physical and biological coupling processes, polynyas of the Amundsen Sea could act as sentinels of changes in atmosphere–ice–ocean interactions, offering a unique perspective into its sensitivity to climate variability. Here, we present a new, multiproxy-based high-resolution sedimentary record from the Amundsen Sea polynya, which provides new insights into environmental conditions of the region over the last 350 years and their linkages to climatic factors. Our results show that the polynya witnessed step-wise environmental shifts in parallel with the phases and strength of large-scale climate patterns, i.e., the Southern Annular Mode (SAM) and El Niño–Southern Oscillation (ENSO). Notably, intersite correlation of on-shelf Circumpolar Deep Water (CDW) intrusion signals at different locals suggests that the CDW may have gained increased access to the shelves at the time of a strong coupling of positive SAM and El Niño states. We tentatively speculate that anomalous large-scale atmospheric and oceanic circulation patterns over the Southern Hemisphere, forced by increasing greenhouse gas levels, were strongly involved in the mid-20th century CDW invigoration, which may be greater in scale that goes well beyond the Amundsen Sea region. This result is relevant to the current debate on spatial heterogeneity in the timing and phasing of major climatic events in Antarctica, underscoring an unambiguous connection of the Antarctic climate state to the large-scale ocean–atmosphere reorganizations. Our study also extends a growing evidence that today's global warming trend is expected to have a severe effect on future configuration of Antarctic continental ice-shelf environment.

1. Introduction

The Amundsen Sea hosts the most rapidly thinning ice shelves in Antarctica today, representing one of the largest sources of glacial meltwater draining from the West Antarctic Ice Sheet (WAIS) to the Southern Ocean (Pritchard et al., 2012; Rignot et al., 2013; Jenkins et al., 2018). With the potential to lead future WAIS collapse (Favier et al., 2014; DeConto and Pollard, 2016), the Amundsen Sea's atmosphere–ocean–ice interaction and its sensitivity to global climate have become a central issue of climate research (e.g., Kimura et al., 2017; Jenkins et al., 2018; Nakayama et al., 2018; Milillo et al., 2019). Studies showed that the continuing ice loss from this region is primarily driven by Circumpolar Deep Water (CDW) intruding onto the Amundsen Sea continental shelf (Rignot et al., 2013; Dutrieux et al., 2014; Paolo et al., 2015). They found that the warm, saline CDW, originated from the southernmost branch of the Antarctic Circumpolar Current, accesses the sub-ice shelf ocean cavity and drives basal ice-shelf melt, ultimately affecting heat and sea-ice distributions over the region. Currently, an increasing number of studies focus on the CDW behavior linked with hemispheric-wide ocean and/or atmospheric circulations that may have implications for major ocean–atmosphere processes in the global climate system (e.g., Dutrieux et al., 2014; Turner et al., 2017; Kimura et al.,

* Corresponding authors.
E-mail addresses: kimsy@kopri.re.kr (S.-Y. Kim), twpark@kopri.re.kr (T. Park).

https://doi.org/10.1016/j.gloplacha.2021.103589
Received 26 January 2021; Received in revised form 30 June 2021; Accepted 23 July 2021
Available online 25 July 2021

2017; Nakayama et al., 2018; Dotto et al., 2020). A particular note is for the two dominant patterns of Southern Hemisphere atmospheric circulation variability: the Southern Annular Mode (SAM) and El Niño–Southern Oscillation (ENSO). Some studies emphasized that changes in the SAM and ENSO states strongly affect ocean heat contents over the Amundsen Sea region through modification of the Amundsen Sea low pressure system, influencing local surface air temperature, wind patterns, water mass characteristics as well as sea-ice dynamics (Yuan and Martinson, 2001; Liu et al., 2004; Hosking et al., 2013; Clem et al., 2017). In this view, polynyas along the coast of the Amundsen Sea gain much attention, because their presence and characteristics are shown to be closely linked to the above-described processes (Maqueda et al., 2004; Alderkamp et al., 2012; Arrigo et al., 2015).

The Amundsen Sea polynya is the most biologically productive region in Antarctica, with high net primary production per unit area of 105.4 g C m^{-2} yr^{-1} (Arrigo et al., 2015) and seasonally averaged chlorophyll-*a* estimate of 2.2 ± 3.0 mg m^{-3} (Arrigo and van Dijken, 2003) that are 16% and 40% higher than the Ross Sea polynya, respectively. In recent years, awareness of a strong interconnectivity of the Amundsen Sea polynya to CDW dynamics has increased, particularly in terms of its bio-productivity and -community structure that can be profoundly altered through changes in glacial melt-laden outflows and associated micronutrient supplies (Gerringa et al., 2012; Alderkamp et al., 2012; St-Laurent et al., 2017). Notwithstanding of such highly responsive nature of these polynyas to the phasing of CDW-driven meltwater runoff and associated hydrographic changes, there is only limited knowledge of mechanisms behind their interactions. Especially, longer-term perspectives on the Amundsen Sea polynya's physical-biological coupling processes are even less constrained due to the paucity of in situ observational datasets with sufficient temporal coverage, although a sound understanding of its temporal variability responding to changing climatic conditions can provide important insights into the present-day and future trends thereof (e.g., Hillenbrand et al., 2017; Lamping et al., 2020).

Here we present multiproxy-based sedimentary records from the Amundsen Sea polynya in order to reconstruct temporal variations in physical-biological parameters of the region over the last ca. 350 years, and to depict major shifts of the environmental regime and their probable linkages to climatic forcing factors. We focus on two distinct climate epochs: the Little Ice Age (LIA) roughly between ca. 1500–1800 CE (Grove, 2004; Paasche and Bakke, 2010) and the modern warm period (post-industrial era, ~present). This time frame is believed to have witnessed the last phase of the LIA – a nearly global, cold climate state caused by natural forcing, followed by a pronounced shift towards modern warming under a strong influence of anthropogenic factors (Masson-Delmotte et al., 2013). Particular emphasis is made on identifying key processes that regulate; 1) glacially-derived micronutrient (i.e., iron) supplies to the study site, and its potential contribution to biological production during major environmental transitions, and 2) an abrupt change in sedimentary redox state centered at the early 1970s and its possible causes.

2. Materials and methods

2.1. Sampling and geochemical analysis

A sediment core was obtained with a box corer from the Amundsen Sea during the Icebreaker ARAON Expedition ANA08B in 2018 (Fig. 1).

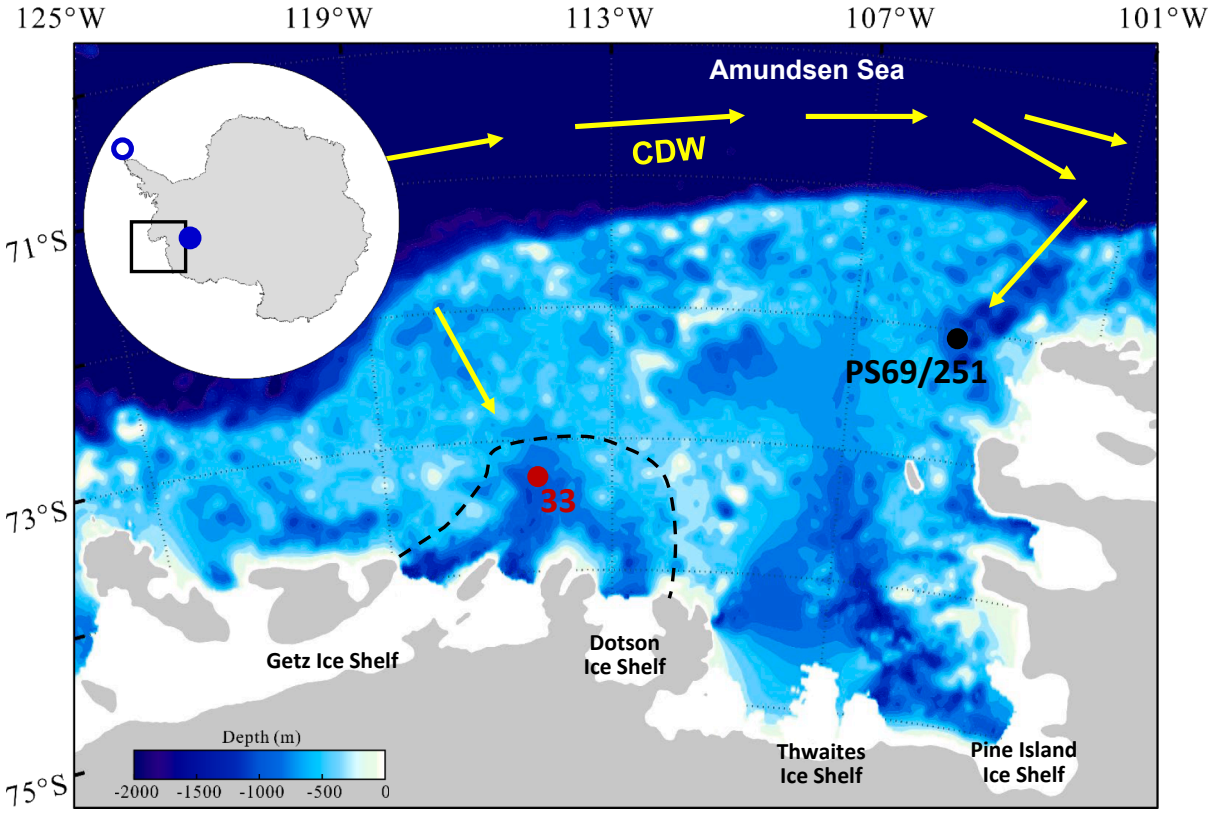

Fig. 1. Map of the Amundsen Sea (black rectangle in inset map), showing the locations of marine sediment core ANA08B/33 (core 33 in the text; red circle), the nearby sediment core PS69/251 (Hillenbrand et al., 2017; closed black circle) from the outer Amundsen Sea shelf, and locations of sites discussed in the text; West Antarctic Ice Sheet Divide deep ice core (Koffman et al., 2014; closed blue circle) and sediment cores from Bransfield Strait, Antarctic Peninsula (Vorrath et al., 2020; open blue circle). Summer polynya boundary is marked by dashed black line (after Kim et al., 2016). Yellow arrows indicate the flow direction of Circumpolar Deep Water (CDW) onto the continental shelf through troughs in the shelf. (For interpretation of the references to colour in this figure legend, the reader is referred to the web version of this article.)

Core ANA08B/33 (hereinafter called core 33) was collected from inside the Amundsen Sea polynya (73.28°S, 114.95°W; 827 m water depth; 50 cm in length). For geochemical composition analysis, the sediment core was subsampled at 1 cm intervals and each subsample was processed using the following procedure. Total carbon (TC) and total sulfur (TS), total inorganic carbon (TIC) concentrations of the subsamples were measured using a CHN elemental analyzer (FLASH 2000; Thermo Fisher Scientific, Waltham, MA, USA) and a CO_2 coulometer (model CM5014; UIC, Joliet, IL, USA), respectively. The analytical accuracy and precision of these elements were within 5%, based on an analysis of standard reference materials (L-cysteine in TC analysis and calcium carbonate with 12.00C% in TIC analysis) and replicated samples. Total organic carbon (TOC) was calculated as the difference between TC and TIC concentrations. Biogenic silica (BSi) concentrations were measured using a wet alkaline extraction method modified from Mortlock and Froelich (1989) and Müller and Schneider (1993). Relative error of the BSi concentration was less than 10%, based on an analysis of standard reference materials – Sodium Silicofluoride (Na_2SiF_6) and silica gel (SiO_2 $2H_2O$) – and replicate samples. BSi concentrations were converted to biogenic opal concentrations based on a weight percentage, using a multiplication factor of 2.14.

To measure element concentrations, each powered sediment sample was fused with lithium metaborate flux and the molten beads were then poured into a volume of dilute nitric acid and stirred until dissolved. The resultant solutions were then analyzed using a combination of a Thermo ICAP 6500 radial ICP-OES and Thermo Elemental X Series II ICP-MS. Calibration for both instruments was achieved via matrix matched calibration standards produced from combinations of ICP-grade single element standards. The accuracy of the analytical method was monitored by repeated analysis of standard reference materials (ACE, OU6 and SBC-1, $n = 5$, respectively), together with a batch of sediment samples. The results showed that relative deviations between measured and certificated values were less than 10%.

2.2. Diatom analysis, diatom-based transfer function and additional datasets

Based on variations of biogenic opal contents, sub-samples for diatom analysis were selected from several sediment intervals of core 33. Diatom analysis was performed at the Chilean Antarctic Institute (INACH), Punta Arenas, Chile, using a microscope (Carl Zeiss model Axio Lab.1 with camera) at 1000 × magnification. Quantitative diatom slides were prepared according to Schrader and Gersonde (1978): cover slips were adhered to the slides using Norland Optical Adhesive #61 (refractive index 1.56) and cured with UV light for at least 30 min. For each slide, a minimum of 400 diatom's valves were counted. Diatom identification followed Armand and Zielinski (2001), Taylor et al. (2001), Crosta et al. (2004), Buffen et al. (2007), Cefarelli et al. (2010), Esper et al. (2010), Allen (2014) and Campagne et al. (2016). The subgenus *Hyalochaete* of the genus *Chaetoceros* were identified as vegetative cells and resting spores. In the case of the species *Thalassiosira antarctica*, two different morphological types were distinguished following Taylor et al. (2001) – T1 associated with colder condition, and T2 as indicators of open water conditions.

In order to estimate Summer Sea Surface Temperature (SSST), we applied the Imbrie and Kipp Method (IKM; Imbrie and Kipp, 1971) and for Winter Sea Ice (WSI) concentration the Modern Analog Technique (MAT; Hutson, 1980). Statistical details and background of the methods and their performance at different application levels, also compared to other estimation methods, are presented in Esper and Gersonde (2014a, 2014b). Estimates of SSSTs were accomplished using TF IKM-D336/29/3q, comprising 336 reference samples from surface sediments in the western Indian, the Atlantic and the Pacific sectors of the Southern Ocean, with 29 diatom taxa and taxa groups, and a 3- factor model calculated with quadratic regression. The SSST estimates refer to summer (January–March) temperatures at 10 m water depth averaged over a time period from 1900 to 1991 (Hydrographic Atlas of the Southern Ocean; Olbers et al., 1992). For estimation of WSI concentrations we applied the transfer function MAT-D274/28/4an which comprises 274 reference samples with 28 diatom taxa/taxa groups and considers an average of 4 analogues (Esper and Gersonde, 2014b). The analogues refer to surface sediments from the Atlantic, Pacific and western Indian sectors of the Southern Ocean. The WSI renders the sea-ice concentrations in a 1° by 1° grid for the September average of the time from 1981 to 2010 (National Oceanic and Atmospheric Administrations; Reynolds et al., 2002, 2007). The threshold of an open ocean to sea-ice covered area is set on 15% of sea-ice concentration (Zwally et al., 2002) and the average sea-ice edge is defined at 40% (Gloersen et al., 1993). The qualitative estimation of sea-ice concentration was derived by the abundance pattern of diatom sea-ice indicators (Gersonde and Zielinski, 2000). The calculations were done with the software R (R Core Team, 2017) using the packages Vegan (Oksanen et al., 2012) and Analogue (Simpson and Oksanen, 2012).

In addition, to compare our results with the large-scale atmospheric circulation variabilities, we used the paleo- El Niño–Southern Oscillation (ENSO) index from Emile-Geay et al. (2013) and the reconstructed Southern Annular Mode (SAM) data from Abram et al. (2014).

2.3. Chronology

Due to the scarcity of foraminiferal specimens in marginal sediments of the Amundsen Sea and problems with the effects of the old carbon reservoir ages in this area (Kim et al., 2016), we used the ^{210}Pb chronology. The geochronology was based on the radioactive decay of ^{210}Pb, which considers the unsupported activities or "in excess" over the background activities, in equilibrium with ^{226}Ra. The CRS model (Constant Rate of Supply; Robbins and Herche, 1993) was chosen to estimate the age at each sediment core section under assumption of a constant ^{210}Pb flux to the sediments, which shows a good agreement with the bulk density distribution of the core sediment (Kim, 2020). The calculations were based on unsupported ^{210}Pb inventories according to Turekian et al. (1980): $t_z = \ln(Q_0/Q_z)/\lambda^{210}$, where t_z is the age at any depth, Q_0 is the excess ^{210}Pb inventory in the core (dpm cm^{-2}), calculated as $\Sigma A_i \rho_i h_i$, where h is the thickness of the interval (cm), Q_z is the excess ^{210}Pb inventory below depth z, A_i is the excess ^{210}Pb activity, and λ^{210} is the decay constant (0.031 y^{-1}). The unsupported value was estimated from the activities at deep core sections (below 24 cm), obtaining similar values reported for the area (4.9 ± 0.2 dpm g^{-1}) at around 18 cm, which is also in agreement with previous studies (2–7 dpm g^{-1} at 6–21 cm; DeMaster and Cochran, 1982; Langone et al., 1998; Masqué et al., 2002; Kim et al., 2016) (Table 1).

The sedimentation rate (v) and mass accumulation rate (r) were estimated according to Christensen (1982) based on the bulk density distribution of the sediment core in the absence of mixing: $\rho = \rho_0 - \rho_1 e^{-az}$; $A = A_0 \exp(-\lambda/r[\rho_0 z - (\rho_1/a)(1 - e^{-az})])$, where $r = \rho v$, ρ is the bulk density (g cm^{-3}), ρ_0 is the bulk sediment density at infinite depth, ρ_1 is the difference between the surface and the deep value, a is the compaction coefficient, and z is the sediment depth. The densities and activities showed a good fit distribution obtaining significant values for all parameters ($p << 0.01$, $R^2 = 0.98$). The accumulated excess ^{210}Pb inventory from the CRS model exhibit a substantial decrease at 12 cm; however, the supported activities were only reached at 18 cm when considering the exponential decay and compaction. Thus, the missing activities between 12 and 18 cm can be predicted from the model fitting, resulting in values closer to the background (or supported activities). Although these activities may have considerable uncertainties, this afforded better excess ^{210}Pb inventory estimations for the upper part of the core (Fig. 2).

3. Results

The ^{210}Pb activities at the surface were higher than those measured

Table 1
Radionuclide activities, depth of unsupported activities (in excess) and sedimentation rates estimated in the Antarctic zone.

References	Lat/Long	Surficial ^{210}Pb activity (dpm g^{-1})	^{226}Ra (dpm g^{-1})	Supported activity estimation (dpm g^{-1})	Depth of excess (cm)	Sedimentation rate (cm y^{-1})
DeMaster and Cochran (1982)	41°–66°S 20°–35°E	21–32	~4–7		8–21	
Masqué et al. (2002)	62°–63°S 59°–60°W	2–21[a]	2–3[a]	2–4[a]		0.060–0.150
Langone et al. (1998)	70°–75°S 165°–170°W				6–10	0.020–0.120
Kim et al. (2016)	71°–74°S 112°–117°W	32[a]		~5[a]	14	0.001–0.013
This study	73.28°S 114.95°W	60		4.9	18	0.09

[a] The reference reports the value in Bq kg^{-1}.

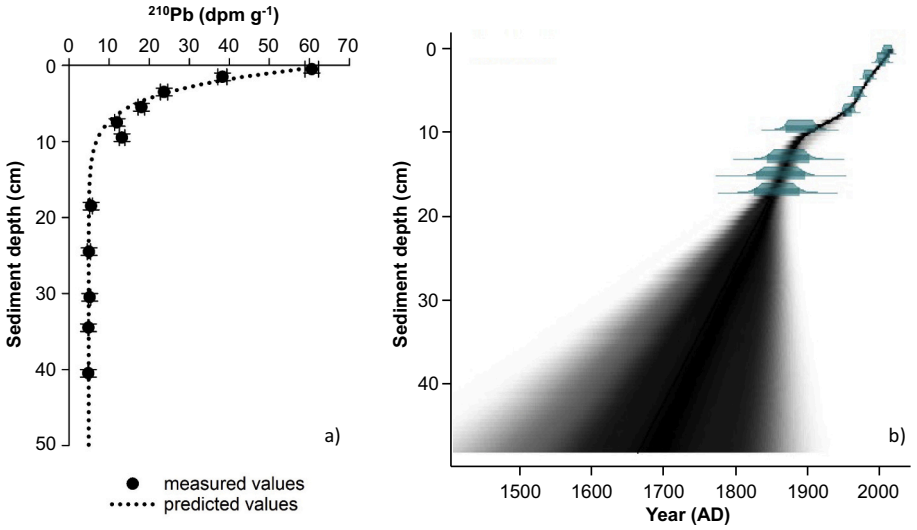

Fig. 2. Chronology of core 33 based on ^{210}Pb excess. The downcore profile of ^{210}Pb (dpm g^{-1}) activity (a) and associated age–depth model with error bars (b).

in Antarctic zones (60 dpm g^{-1}; Table 1), but the mass accumulation rate was in the range of other estimations from the region (0.041 ± 0.004 g cm^{-2}y^{-1}) and the sedimentation rates were in relatively higher range of estimations made at the western of Antarctica (0.09 cm y^{-1}), resulting in an estimated date of ca. 1663 CE at the end of the core (DeMaster and Cochran, 1982; Langone et al., 1998; Masqué et al., 2002; Kim et al., 2016; Table 1). These results indicate that our age estimates are reasonable based on the ^{210}Pb inventories and associated sediment composition changes. In Kim et al. (2016), the sedimentation rates at the periphery and center of the polynya were one order of magnitude higher than the nearest shelf break and nearby ice shelf, due to glacial meltwater discharges and terrigenous matter supplies from nearby ice shelf to the sampling site during warmer climate conditions. The sedimentation rate at this region is considered to be constant, and can be modified primarily by sediment compaction in relation with the bulk density distribution that may affect the estimated ages for the oldest part of the core sediment. Thus, assuming that sediment compaction is the main process involved in the bulk density increase with sediment depth, the constant mass accumulation rates of core 33 allow us to establish reasonable age estimates for sediments older than ~100 years (i.e., below the ^{210}Pb excess or unsupported). In this study, given the limit of the ^{210}Pb method (e.g., Nittrouer et al., 1970; Robbins and Edgington, 1975), the sedimentation rates and age dates below 10 cm are referred to as "approximate".

Probable effects of biological sediment mixing (i.e., bioturbation) by benthic organisms on the ^{210}Pb activity profile cannot be ignored. As is often the case, sediments with intense bioturbation tend to show a uniform ^{210}Pb activity throughout the top few centimeters, as a result of mixing of the higher surface activity of excess ^{210}Pb with deeper sediments containing less ^{210}Pb (Sanders et al., 2010; Jankowska et al., 2016; Serrano et al., 2016). In the core 33 sediments, however, the excess ^{210}Pb activities exhibit an exponentially decreasing trend from the core top down to 10 cm, below which a flattening of the profile occurs as the ^{210}Pb activity reaches background levels. We also note that attenuation of the radioactivity decay by diffusive bioturbation diminishes with depth; it is limited by the fauna biomass, mostly concentrated in a few centimeters below the sediment-water interface at greater water depths (> 200 m, Soetaert et al., 1996). Therefore, the excess ^{210}Pb depth distribution do not seem to indicate a significant impact of bioturbation, allowing for reasonable age estimations based on accumulated inventories of radioactivity below the surface sediments. Diffusive mixing is possible, but its strong interference with the age estimations is unlikely; in our case, the bulk density shows an exponential increase in consider of sediment compaction and the estimated mass sedimentation rates (Christensen, 1982). This inference is consistent with the high carbon rain rates in the study zone, which also reduce a probability of biological mixing interference. Thus, we consider that the activity gradient of core 33 is primarily affected by sediment burial and ^{210}Pb decay, and the effect of bioturbation is expected to be minimal.

TOC, TN, TS and opal contents ranged 0.66–1.15% (average: 0.82%), 0.09–0.17% (average: 0.11%), 0.09–0.22% (average: 0.14%) and 12.21–14.65% (average: 13.14%), respectively. Noteworthy is an abrupt increase in their contents at ~1800 CE. At this time, opal contents, in

particular, show a sharp rise reaching its highest value of 14.65%. After overall fairly consistent trends (ca. 1850–1950 CE), TN, TOC, and TS contents exhibit a remarkable increase commencing at ca. 1960 CE and keep high values onwards. However, opal contents remain relatively high and keep an overall consistent trend, after a sharp decline at ~1800 CE (Fig. 3).

Variations of elemental composition appear to well correspond to the aforementioned step-wise changes in the organic components (Fig. 3). Notably, Al contents remain overall consistent until ca. 1800 CE varying between 8.64% and 9.00% (average: 8.87%), and begin to decrease reaching its modern value of 7.91% at the core top, suggesting general upward-coarsening in sediment grain size (Schropp et al., 1990; Din, 1992). Fe/Al ratios – grain size-normalized contents of Fe – were also held constant until ~1800 CE, followed by a sharp and continuous elevation towards the core top values. Ba/Al ratios steadily increase until around 1850 CE, followed by lowered values from ca. 1850 CE to 1960 CE, with considerably higher values increasing after ~1970 CE. Redox-sensitive element ratios (i.e., Mo/Al, Mn/Al, P/Al and Ni/Al) exhibit overall low and rather muted values until around 1970 CE. However, an abrupt increase commences at 1970–1980 CE and the value remains high towards the core top, being consistent with the TS content patterns (Fig. 3). Together, these features indicate a substantial supply of

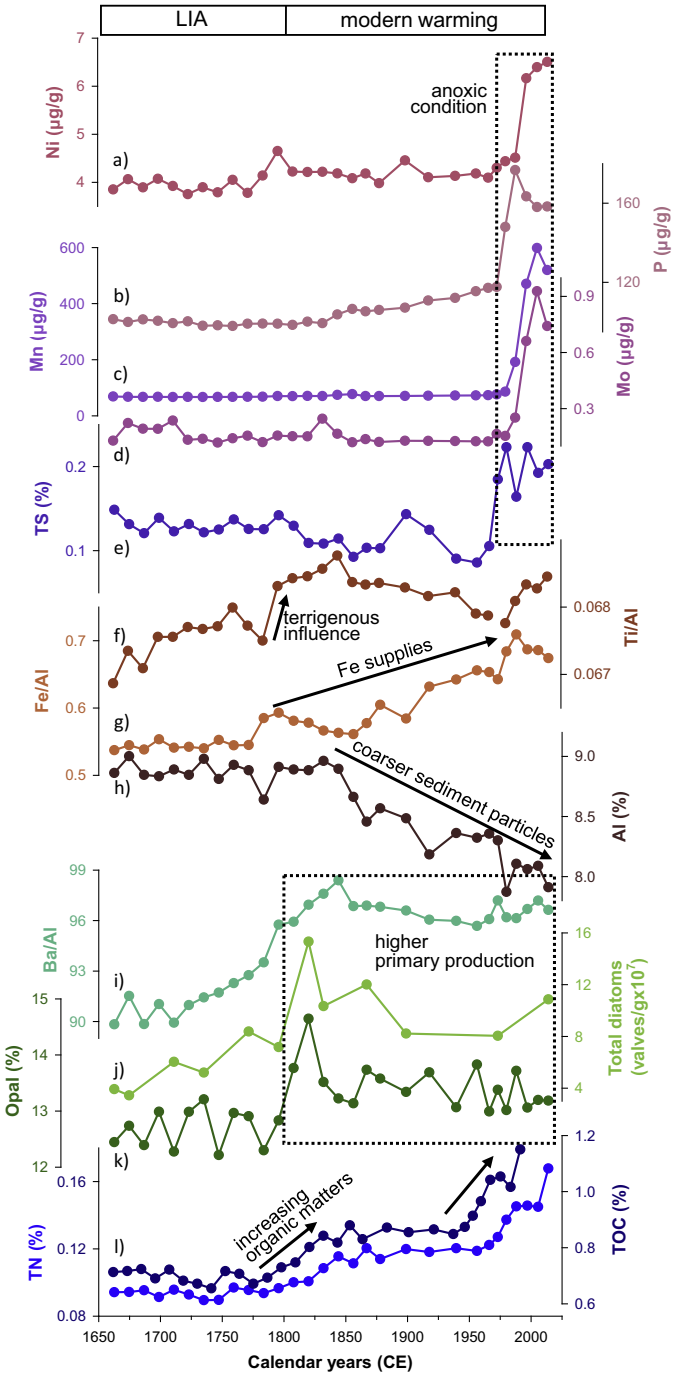

Fig. 3. Proxy records of environmental changes in Amundsen Sea Polynya from core 33; a) Ni content, b) P content, c) Mn content, d) Mo content, e) TS content, f) Ti/Al ratio, g) Fe/Al ratio, h) Al content, i) Ba/Al ratio, j) diatom concentrations, k) biogenic opal content and l) TN and TOC contents.

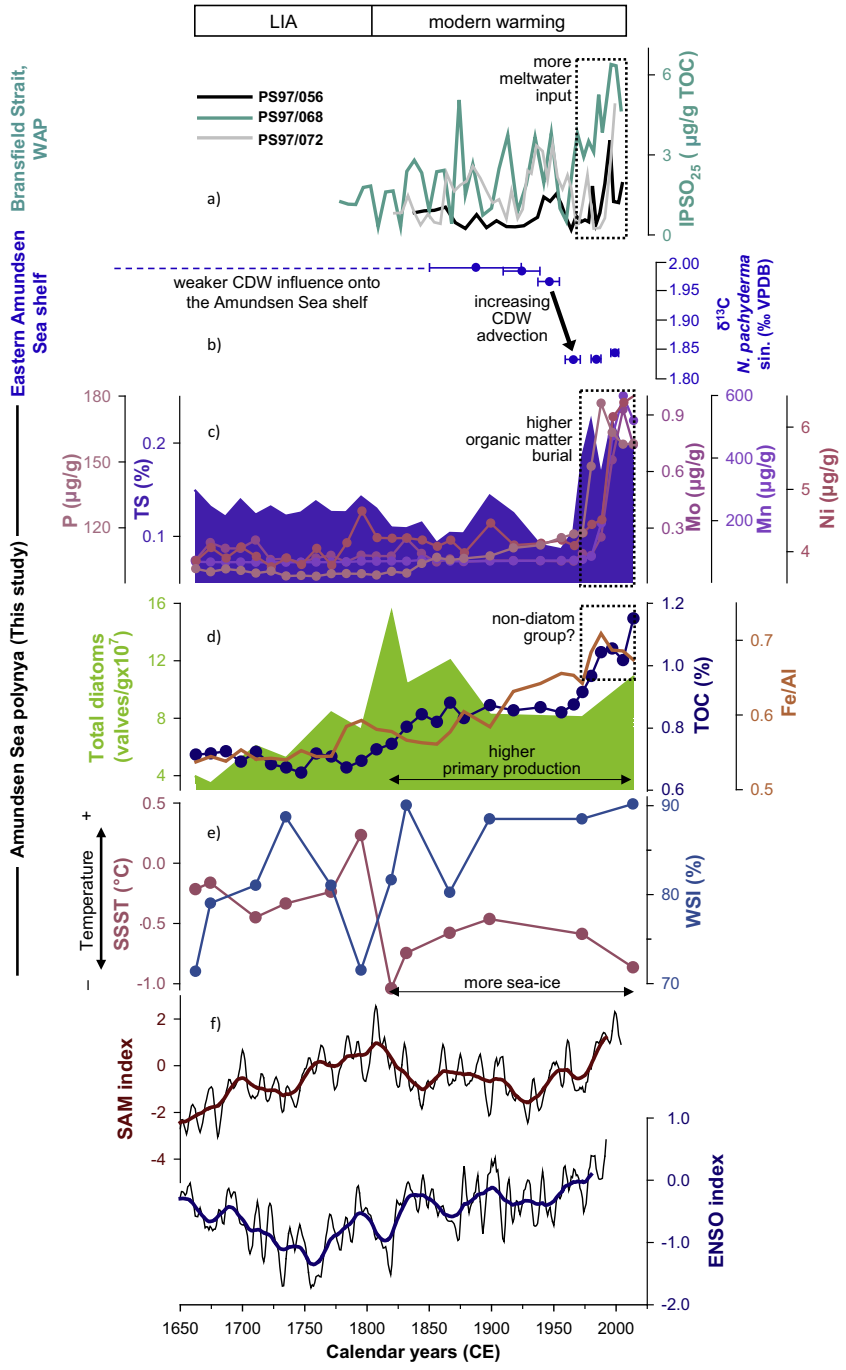

Fig. 4. Compilation of palaeoclimatic records from core 33 (this study) and sediment cores from the West Antarctic shelves, and basic interpretation of major climatic events. (a) concentrations of biomarker $IPSO_{25}$ in sediment cores from the Bransfiled Strait, Antarctic Peninsula (Vorrath et al., 2020). (b) $\delta^{13}C$ values of planktic foraminifer shells in core PS69/251 from the outer Amundsen Sea shelf (Hillenbrand et al., 2017). (c) proxy records of redox-sensitive elements and TS content. (d) proxy records of marine productivity. (e) reconstructed sea surface temperature and sea-ice concentration estimates derived from diatom assemblages. (f) the El Niño–Southern Oscillation (ENSO; Emile-Geay et al., 2013) and the Southern Annular Mode (SAM; Abram et al., 2014) data for the past 400 years. The curves are smoothed by 11-year (thin lines) and 31-year (thick lines) moving averages of yearly indices.

these elements into the coring site since ca. 1970 CE, as with increasing sediment grain size.

A total of 35 diatom species belonging to 18 genera were identified in the core sediment samples. Throughout the core, the most abundant species was *Fragilariopsis curta* (29.0–62.3%, 45.9% on average), followed by *Chaetoceros* resting spore spp. (6.6–38.2%, 19.7% on average), *Thalassiosira antarctica* (T1, morphotype of cold waters; 2.8–10.9%, 6.4% on average), *Eucampia antarctica* var. *recta* (1.4–7%, 4% on average) and *F. vanheurckii* (0–10.35%, 4.14% on average). Absolute diatom abundance – as in the number of diatom valves per gram of dry sediment – remains relatively low until 1796 CE (ca. 34.5–83.8 $\times$ 10^6 g^{-1}, 60 $\times$ 10^6 g^{-1} on average). At around 1800 CE, the total diatom concentration shows an abrupt and rapid rise to its maximum value of >153 $\times$ 10^6 g^{-1}, followed by a somewhat decreasing trend from ca. ~1800 CE to 1970 CE. This abrupt change in diatom abundance coincides with the diatom-derived SSST estimates that shift at ~1800 CE from higher values (−0.45 °C to 0.23 °C, −0.19 °C on average) to distinctly lower values (−1.04 °C to −0.46 °C, −0.71 °C on average). Diatom-based WSI concentration estimates are strongly variable throughout the core (66.46–89.07%, 83.45% on average) but show a pronounced drop at ca. 1800 CE with its lowest value (Fig. 4).

4. Discussion

4.1. A regime shift in the Amundsen Sea shelf environment after the end of the LIA

One of the strongest signals is a series of abrupt changes in various proxies at ~1800 CE (~1800–1830 CE) (Fig. 3), notably represented by a concordant increase in organic matter (e.g., TOC, TN and opal), diatom frustules and Ba contents indicating enhanced marine productivity. This interval is concurrent with a significant transition in trace element contents: here a noticeable rise in Fe and Ti indicates larger amounts of terrigenous matters, whereas a decrease in Al infers higher deposition of coarse-grained particles (Naidu et al., 1997; Xu et al., 2015). Given that trace metals tend to be concentrated in fine-sized sediments (Horne, 1969; Moussa, 1983; Presley, 1997), such opposite behavior of Fe and Ti to the decreasing Al (i.e., sediment coarsening) may suggest inputs of larger particles and terrestrial matters to the site rather than the grain-size effect on adsorption of heavy metals. In the Amundsen Sea coastal regions, magnitudes of phytoplankton growth and primary production are controlled by a complex interplay of water column stability, solar radiation intensity, sea-ice coverage and nutrient concentrations (Arrigo et al., 2003; Gerringa et al., 2012). Particularly, in situ observations highlighted the availability of iron (Fe), an essential micronutrient for algal growth (Krause and Weis, 1991; Falkowski et al., 1992), as a key factor determining high level of phytoplankton biomass in the Amundsen Sea (Arrigo et al., 2015; Sherrell et al., 2015; St-Laurent et al., 2017). Therefore, the increasing biological productivity after ~1800 CE seems to well match with the signal of higher terrigenous micronutrient (i.e., Fe) inputs.

Specific mechanism(s) of such higher deposition of these terrestrial components to the study site after ~1800 CE could involve two major transport pathways. One pathway is associated with atmospheric winds

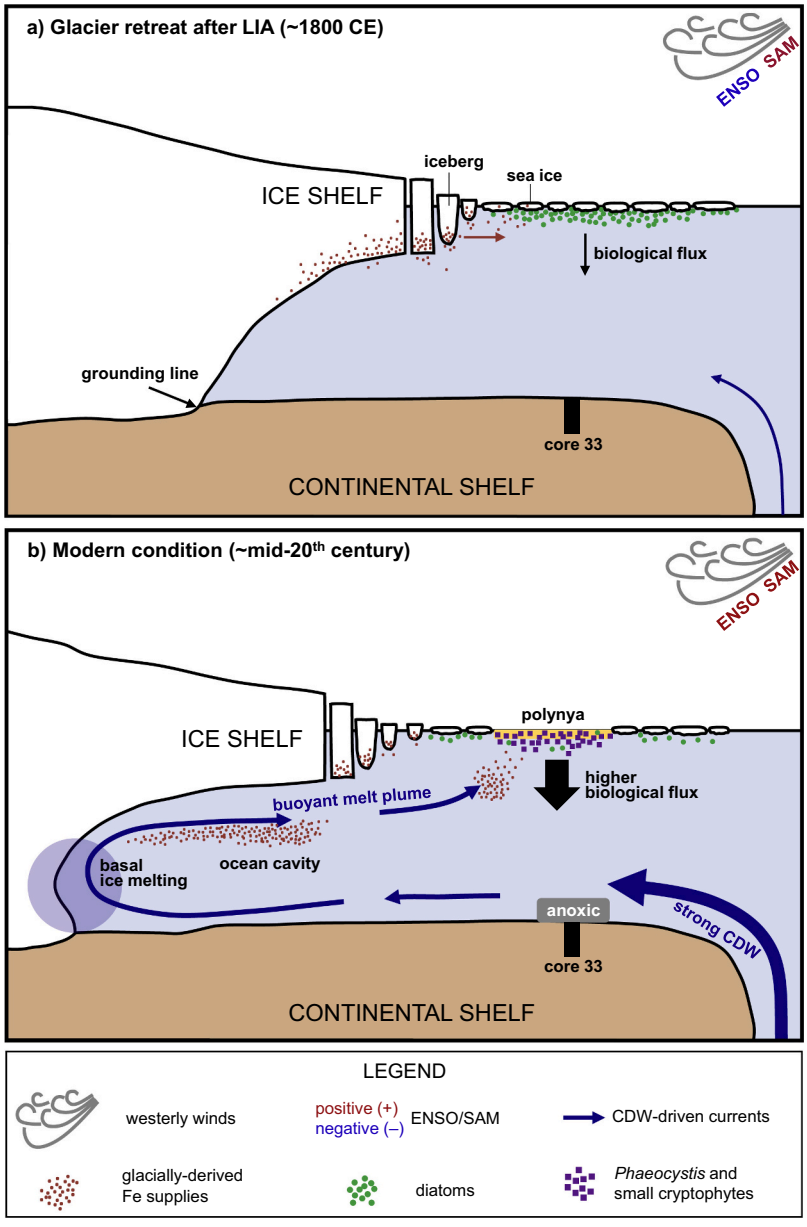

Fig. 5. Schematic illustration of the Amundsen Sea polynya at the West Antarctic continental shelf showing distinct environmental conditions at the 33 core site for selected time intervals; a) after the LIA termination and b) modern condition established after the mid-20th century. The simplified view illustrates major physical processes that can influence marine productivity and phytoplankton community changes.

carrying dust particles from surrounding extra-Antarctic continents (i.e., Australia, South America, and South Africa) to western West Antarctica (Li et al., 2008; De Deckker et al., 2010; Mahowald et al., 2010). However, terrestrial dust flux and particle size data from the West Antarctic Ice Sheet Divide deep ice core (Koffman et al., 2014; for location see Fig. 1) show reduced dust deposition and coarse particle transport to West Antarctica after the end of the LIA, indicating a weakened circumpolar westerly wind strength. Therefore, a contribution of wind-transported terrestrial matters was unlikely significant at the time. The other pathway is associated with icebergs, one of the most important suppliers of Fe in the Southern Oceans (Raiswell et al., 2008; Duprat et al., 2016; Schwarz and Schodlok, 2009). Especially, sediments released from the icebergs contain much higher amounts of ferrihydrite (highly bioavailable Fe nanoparticles) than atmospheric dust, and are regarded as a more effective Fe fertilizer (Raiswell et al., 2016). It appears, therefore, conceivable that the increased Fe contents in our core data may indicate more supplies of icebergs that are shed from nearby ice shelf front, fertilizing the shelf waters with sufficient bioavailable Fe released from the melting icebergs.

The inferred iceberg discharge event after ~1800 CE, almost corresponding to the end of the LIA, may require further explanation. Although currently a very small-sized ice shelf exists in the Amundsen Sea sector of the WAIS today, geologic data and numerical models suggest a massive extending of the ice at this region, with episodes of rapid retreats and re-advances, during some periods of its climate history (e.g., Kirshner et al., 2012; Larter et al., 2014; Klages et al., 2017). Despite the fact that reliable reconstructions of past ice sheet configuration during the LIA are still lacking for many WAIS sectors, there are finds of strong evidence for LIA glacial advance and ice shelf expansion in the Southern Hemisphere high latitude regions – for instance, the Antarctic Peninsula (Domack et al., 1995; Brachfeld et al., 2003; Christ et al., 2015), southern South America (Koch and Kilian, 2005; Strelin et al., 2008) and Southern Alps of New Zealand (McKinzey et al., 2004; Winkler, 2009). Tentatively, we propose that glacial advance with a large ice shelf development in the Amundsen Sea region during the LIA and its subsequent retreat or deterioration may explain the iceberg discharge signature at ~1800 CE in core 33. If correct, such a climatic transition would have invoked not only a large supply of broken ice pieces shed from the ice-shelf front delivering large-size particles to coastal areas, but also substantial changes in hydrodynamic condition at the site. This speculation is corroborated by the diatom-derived WSI and SSST estimates, which exhibit sudden and unusual fluctuations at ~1800 CE (Fig. 4). A particular note is for a sharp decrease in the paleo-SSST, which seems to deviate from the timing of post-LIA climate amelioration postulated here. Clues about it may be drawn from recent observational studies, which show that discharges of glacial meltwater from the Antarctic ice shelves result in cooling of the surface coastal water, owing to the meltwater-induced surface freshening and stratification (Bronselaer et al., 2018). Thus, the seemingly opposite behavior of the SSST change can be well reconciled with our hypothesis of LIA ice shelf growth and subsequent reduction over the Amundsen Sea region. That rather unstable state of sea surface conditions, along with more open marine influences on the site, is likely to stimulate phytoplankton population growth there (Xiao et al., 2013 and references therein). Considering all the above, it is conceivable that post-LIA iceberg and meltwater discharges with more seasonally open-marine conditions possibly stimulated growth of diatom groups that have an affinity for cold temperature and sea-ice conditions (Smith Jr. and Comiso, 2008; Taylor et al., 2013; Wang et al., 2014), while other phytoplankton groups were not able to tolerate the overall hostile habitat condition.

Such concerted changes in the sediment data after ~1800 CE, inferring a possibility of the post-LIA ice shelf deterioration, seem to relate in time to the reconstructed ENSO and SAM patterns. After a continuous rise since ca. 1650 CE, the positive trend in the SAM reaches its maximum values in the early 1800s when the ENSO displays a strong negative polarity (Fig. 4). Observational studies show that a positive SAM alters sea-ice and air temperature conditions across the West Antarctic region, by shifting the Southern Hemisphere westerly winds southward (Marshall, 2003; Dixon et al., 2011; Koffman et al., 2014). Also, it was shown that regional wind patterns at the Amundsen Sea are strongly affected by a low-pressure system over the Ross and Amundsen-Bellingshausen Seas (i.e., Amundsen Sea Low) that tends to be deepened during a La Niña period, with the tropical-extratropical Pacific forcings playing a part (Yuan, 2004; Turner et al., 2017 and references therein). Such atmospheric anomalies over the Amundsen Sea responding to the tropical Pacific influence are further intensified when a strong positive SAM coincides with La Niña, resulting in surface cooling and stronger southerly winds from the continental interior associated with lowered air pressure (Yuan and Martinson, 2001; Liu et al., 2004; Stammerjohn et al., 2008). If our interpretation of the ice shelf decay and the resultant iceberg discharges after ~1800 CE discussed in the preceding section is correct, the strengthened southerly winds from the continent would tentatively facilitate equatorward dispersion of icebergs from the ice-shelf. Taken as a whole, we speculate that the post-LIA climate amelioration in concert with a combined effect of the two severe climate modes may have invoked considerable transitions in the ice–atmosphere–marine state at the region after ~1800 CE. This may involve more open ocean conditions with large supplies of icebergs and micronutrient (Fe) inputs from the receding ice shelf front, stimulating production of phytoplankton groups with high tolerance to such hostile habitat condition (Figs. 4 and 5a).

After ~1800 CE onward, a pause in the post-LIA marine productivity increase is indicated by proxy data such as organic matter, Ba/Al ratios, diatom frustules and opal contents (Fig. 3). This pattern is contemporaneous with overall halted trends of the diatom-derived SSST and WSI records after the large fluctuation at ~1800 CE (ca. 1800–1830 CE), indicating relatively stabilized sea surface conditions with lowered sea surface temperatures and more sea-ice abundance (Fig. 4). Further, relatively subtle variations of the ENSO–SAM indices from ~1800 until ~1970 CE seem to match with the marine productivity that stayed on since ~1800 CE (Fig. 4). Such general similarities between all these features may infer a continuation of the shifted atmospheric circulation patterns after the mid-19th century, probably affording stabilized regional sea-ice conditions and oceanic water mass properties, as well as overall habitat conditions for phytoplankton population growth there. For this time interval, Al contents and Fe/Al ratios keep its decreasing- and increasing trends, respectively, since ~1800 CE (Fig. 4). This may suggest that the ice shelf break-up and glacial meltwater discharges had not stopped or weakened since the termination of the LIA, ensuing continued supplies of terrestrial matters including micronutrients to the shelf waters.

4.2. *Present-day polynya development and timing of the CDW enhancement*

After around 1970 CE, a strong signature of environmental changes arises from very abrupt and steep elevations in a series of redox-sensitive elements (i.e., Ni, P, Mn and Mo) as well as TS contents (Fig. 4). In general, these trace element behaviors in marine sediments provide valuable information regarding chemical state of depositional environments (Calvert and Pedersen, 1993). Particularly, such a sharp increase of redox-sensitive elements can be indicative of anoxic or significantly oxygen-depleted conditions in bottom water and upper sediment layer (e.g., Morford and Emerson, 1999; Lim et al., 2011; Muñoz et al., 2012), primarily ascribed to higher biological productivity and/or lowered bottom-water oxygen conditions during deposition of the sediments (e.g. Diaz, 2001; Wallace et al., 2014). However, a drastic bottom-water renewal event in the study region is unlikely, because a strong oxygen-depleted water mass formation is typically subjected to occur in environments with restricted deep-water exchanges (e.g., silled basin) (Rabalais et al., 2010; Friedrich et al., 2014). Therefore, the alleged redox proxy signal after ~1970 CE in our core suggests much higher

primary production and organic matter burial fluxes at the time period, enhancing O_2 consumption within the sediments due to oxidation of the organic matters. This interpretation gains support from concordant elevations in TOC and TN contents, along with Fe/Al and Ti/Al ratio data that indicate a continuation of terrestrial matter supplies to the site (Fig. 4).

Despite the aforementioned signals inferring a rebound in marine productivity after ~1970 CE, the diatom-derived indices (i.e., total diatom concentration and biogenic opal contents, as well as the SSST and WSI estimates) exhibit rather subtle changes. Clues about it might be drawn from phytoplankton community responses to environmental changes that differ greatly depending on various groups and individual species (Rose et al., 2009; Xu et al., 2014). In the Amundsen Sea shelf coastal water today, massive recurrent blooms in the surface waters are primarily fostered by prymnesiophytes (mainly *Phaeocystis antarctica*) and small cryptophytes, as well as diatoms (Tortell et al., 2012; Delmont et al., 2014; Kim et al., 2017; Lee et al., 2016). Thus, the rather muted signal of our diatom-derived proxies probably signifies a substantial transition in the local phytoplankton community after ~1970 CE, probably driven by accelerating glacial meltwater inputs and freshening of coastal surface waters (Moline et al., 2004; Peloquin and Smith Jr., 2007; Sedwick et al., 2007). Such situation may have acted in a way that has promoted much higher primary production of soft-bodied and unfossilizable phytoplankton groups that cannot be captured in our sediment records.

Based on these results, the fundamental question we raise is how such strong perturbations in the local biological environment can be possibly induced. In this regard, a particular note is for the recent observations, which show rapid melting of floating ice shelves, meltwater outflow acceleration and grounding-line retreat in the Amundsen Sea initiating at the early 1970s (Sutterley et al., 2014; Mouginot et al., 2014; Rignot et al., 2014). Instrumental data from the Dotson ice shelf, nearby the coring site under study, also display concordant signals in glacial melt rates, grounding-line position, and incised channel geometry, inferring that a pronounced glacier retreat began in the early 1970s or before (Lilien et al., 2018). What becomes apparent is a crucial role of the CDW intrusion to the shelf in driving such a rapid ice loss and bioessential micronutrient supplies into the shelf waters (Rignot et al., 2013; Sherrell et al., 2015; St-Laurent et al., 2017), leading to the present day's high productivity level in this region. This view includes thoughts for its influence on the sustained high phytoplankton growth; not only by supplying particulate iron and other nutrients (Schofield et al., 2015; St-Laurent et al., 2017), but also by developing the meltwater-driven hydrographic structure that ensures more favorable habitat conditions (Alderkamp et al., 2012). The latter process has been highlighted as an additional determining factor for coastal polynya formation, besides the offshore-flowing katabatic wind as a primary factor. That is, the CDW-induced glacial meltwater outflow reaches the open-surface water with sufficient residual heat and buoyancy, and melts the sea-ice, ultimately preventing further fast ice formation and thus stimulating polynya development at the location (Mankoff et al., 2012; Alley et al., 2016). Considering all the above, it is conceivable that the enhanced on-shelf CDW intrusion since the early 1970s may have resulted in pervasive meltwater-driven oceanographic changes and more extensive polynya formation in the Amundsen Sea region today, affording greater biological production and phytoplankton community shift (Figs. 4 and 5b).

From a climatic point of view, we focus on a strong positive swing in the SAM and ENSO after ca. 1950 CE, where both indices are synchronous to higher values (Fig. 4). It has been shown that a positive trend of the SAM during the recent decades is ascribed to enhanced meridional temperature gradients in the Southern Hemisphere, owing to Antarctic ozone depletion and emissions of greenhouse gases (Marshall, 2003; Thompson et al., 2011; Gillett and Fyfe, 2013; Abram et al., 2014). Paleoclimate data of Li et al. (2013) also revealed that El Niño variabilities in the late 20th century was "unusually active", probably in responding to increasing anthropogenic radiative forcing. Further, more extreme El Niño events in the tropical Pacific are predicted, as a consequence of a weakening of both equatorial (east–west) and meridional (equator to mid-latitudes) sea surface temperature gradients, and reorganization of atmospheric convection (Cai et al., 2014; Abram et al., 2014). Such contemporaneous rises in positive SAM and El Niño conditions tend to intensify anomalous eastward flow over the continental shelf break, thereby strengthening the CDW advection onto the shelf (Thoma et al., 2008; Stammerjohn et al., 2015 and references therein; Turner et al., 2017). Therefore, it is possible that increasing on-shelf CDW influence since the mid-20th century with its substantial contribution to sustained heat and freshwater supplies into surface waters (Mankoff et al., 2012; Dutrieux et al., 2014; Paolo et al., 2015; Alley et al., 2016) played a pivotal role in shaping present-day polynya environment of the study region and biological production therein.

We further hypothesize that, the CDW invigoration since the mid-20th century under a probable influence of anomalous greenhouse-driven climatic patterns over the Southern Hemisphere, may be greater in scale that goes well beyond the study area. This inference is supported by the *N. pachyderma* sin.-derived $\delta^{13}C$ ratio data from the outer Amundsen Sea shelf (core PS69/251), which indicate that the current mode of CDW intensification was established at between ca. 1950–1960 CE (Hillenbrand et al., 2017; for location see Fig. 1). Interestingly, the timing of the CDW advection growth in the Amundsen Sea shelf evidenced here coincides with those identified in the Bransfield Strait, the western Antarctic Peninsula (Vorrath et al., 2020; for location see Fig. 1). In the study, a strong increase in CDW and the Bellingshausen Sea Water (BSW) intrusions to the Bransfield Strait since the 1970s has been captured by the sea-ice biomarker proxy data (e.g., $IPSO_{25}$; Fig. 4). The biomarker-based sea-ice estimates indicate a rapid sea-ice advance at coastal sites of the region during the time of increasing on-shelf influence of these warm waters – the process primarily involves larger meltwater discharges from retreating glaciers and subsequent strong stratification of the water column, thereby promoting more sea-ice formation due to higher freezing point of freshwater. Collectively, all these combined sedimentary data from different locations lead us to tentatively speculate that the CDW has gained increased access to the shelves since the mid-20th century, at the time of a strong coupling of positive SAM and El Niño states. We note that reliable reconstructions on past dynamics of these air–ocean–ice processes are still lacking for many West Antarctic regions and therefore, further in-depth investigations are needed to explain the underlying mechanism of the observed phenomena.

5. Conclusions

Our multiproxy dataset suggests that the Amundsen Sea polynya experienced step-wise changes over the past 350 years, following climatic transitions from the late LIA to the modern warming (post-industrial) period: 1) a strong increase in marine productivity related to higher glacier-derived Fe supplies from ice shelf break-up after the termination of the LIA (~1800 CE), 2) a rather paused biological productivity with overall stabilized oceanographic conditions for the phytoplankton growth (~1800–1970 CE), and 3) intensive polynya formation after the establishment of the current mode of on-shelf CDW inflow (after ~1970 CE), affording greater phytoplankton biomass and a marked shift in the local biological community.

We associate the chain of events outlined above with the large-scale atmospheric circulation patterns represented by SAM and ENSO phases. In particular, increased iceberg discharges and marine biological production (mainly sea-ice diatoms) after ~1800 CE probably infer the post-LIA ice shelf deterioration under a strong positive SAM reinforced by a La Niña condition. Further, the mid-20th century's CDW invigoration signatures at different locals, in concert with the recent anomalous large-scale climate patterns over the Southern Hemisphere, may suggest a pervasive and greater-scale transmittance of anthropogenic

greenhouse-gas forcings into the West Antarctic ice shelf system. Considering the limited scientific data for the Antarctic region, more research with widespread data collections is needed to better understand palaeodynamics of the Antarctic climate system and their linkages to the large-scale ocean–atmosphere reorganizations.

Declaration of Competing Interest

The authors declare that they have no known competing financial interests or personal relationships that could have appeared to influence the work reported in this paper.

Acknowledgement

We are grateful to the captain and crew of the RV ARAON for their assistance with collection of the sediment core sample used. This study is a contribution to the Korea Polar Research Institute research program under grant no. PE21110. We also thank the 'Ecosystem Structure and Function of Marine Protected Area (MPA) in Antarctica' project (PM21060), funded by the Ministry of Oceans and Fisheries (20170336), Korea. The authors wish to thank three anonymous reviewers and the editor (F. Marret-Davies) for their constructive comments improving the manuscript.

References

Abram, N.J., Mulvaney, R., Vimeux, F., Phipps, S.J., Turner, J., England, M.H., 2014. Evolution of the southern annular mode during the past millennium. Nat. Clim. Chang. 4, 564–569. https://doi.org/10.1029/2002PA000846.

Alderkamp, A.C., Mills, M.M., van Dijken, G.L., Laan, P., Thuróczy, C.-E., Gerringa, L.J. A., de Baar, H.J.W., Payne, C.D., Visser, R.J.W., Buma, A.G.J., Arrigo, K.R., 2012. Iron from melting glaciers fuels phytoplankton blooms in the Amundsen Sea (Southern Ocean): Phytoplankton characteristics and productivity. Deep-Sea Res. II 71-76, 32–48. https://doi.org/10.1016/j.dsr2.2012.03.005.

Allen, C.S., 2014. Proxy development: a new facet of morphological diversity in the marine diatom *Eucampia antarctica* (Castracane) Mangin. J. Micropalaeontol. 33 (2), 131–142. https://doi.org/10.1144/jmpaleo2013-025.

Alley, K.E., Scambos, T.A., Siegfried, M.R., Fricker, H.A., 2016. Impacts of warm water on Antarctic ice shelf stability through basal channel formation. Nat. Geosci. 9, 290–294. https://doi.org/10.1038/ngeo2675.

Armand, L.K., Zielinski, U., 2001. Diatom species of the genus *Rhizosolenia* from Southern Ocean sediments: distribution and taxonomic notes. Diatom Res. 16 (2), 259–294. https://doi.org/10.1080/0269249X.2001.9705520.

Arrigo, K.R., van Dijken, G.L., 2003. Phytoplankton dynamics within 37 Antarctic coastal polynya systems. J. Geophys. Res. 108 (8), 3271. https://doi.org/10.1029/2002jc001739.

Arrigo, K.R., Worthen, D.L., Robinson, D.H., 2003. A coupled ocean-ecosystem model of the Ross Sea: 2. Iron regulation of phytoplankton taxonomic variability and primary production. J. Geophys. Res. 108 (C7), 3231. https://doi.org/10.1029/2001JC000856.

Arrigo, K.R., van Dijken, G.L., Strong, A.L., 2015. Environmental controls of marine productivity hot spots around Antarctica. J. Geophys. Res. Oceans 120, 5545–5565. https://doi.org/10.1002/2015JC010888.

Brachfeld, S., Domack, E., Kissel, C., Laj, C., Leventer, A., Ishman, S., Gilbert, R., Camerlenghi, A., Eglinton, L.B., 2003. Holocene history of the Larsen-A Ice Shelf constrained by geomagnetic paleointensity dating. Geology 31, 749–752. https://doi.org/10.1130/G19643.1.

Bronselaer, B., Winton, M., Griffies, S.M., Hurlin, W.J., Rodgers, K.B., Sergienko, O.V., Stouffer, R.J., Russell, J.L., 2018. Change in future climate due to Antarctic meltwater. Nature 364, 53–58. https://doi.org/10.1038/s41586-018-0712-z.

Buffen, A., Leventer, A., Rubin, A., Hutchins, T., 2007. Diatom assemblages in surface sediments of the northwestern Weddell Sea, Antarctic Peninsula. Mar. Micropaleontol. 62 (1), 7–30. https://doi.org/10.1016/J.MARMICRO.2006.07.002.

Cai, W., Borlace, S., Lengaigne, M., van Rensch, P., Collins, M., Vecchi, G., Timmermann, A., Santoso, A., McPhaden, M.J., Wu, L., England, M.H., Wang, G., Guilyardi, E., Jin, F.-F., 2014. Increasing frequency of extreme El Niño events due to greenhouse warming. Nat. Clim. Chang. 4, 111–116. https://doi.org/10.1038/nclimate.

Calvert, S.E., Pedersen, T.F., 1993. Geochemistry of recent oxic and anoxic marine sediments: implications for the geological record. Mar. Geol. 113, 67–88. https://doi.org/10.1016/0025-3227(93)90150-T.

Campagne, P., Crosta, X., Schmidt, S., Noëlle Houssais, M., Ther, O., Massé, G., 2016. Sedimentary response to sea ice and atmospheric variability over the instrumental period off Adélie Land, East Antarctica. Biogeosciences 13 (14), 4205–4218. https://doi.org/10.5194/bg-13-4205-2016.

Cefarelli, A.O., Ferrario, M.E., Almandoz, G.O., Atencio, A.G., Akselman, R., Vernet, M., 2010. Diversity of the diatom genus *Fragilariopsis* in the Argentine Sea and Antarctic waters: morphology, distribution and abundance. Polar Biol. 33 (11), 1463–1484. https://doi.org/10.1007/s00300-010-0794-z.

Christ, A.J., Talaia-Murray, M., Elking, N., Domack, E.W., Leventer, A., Lavoie, C., Brachfeld, S., Yoo, K.-C., Gilbert, R., Jeong, S.-M., Petrushak, S., Wellner, J., the LARISSA Group, 2015. Late Holocene glacial advance and ice shelf growth in Barilari Bay, Graham Land, West Antarctic Peninsula. Geol. Soc. Am. Bull. 127 (1–2), 297–315.

Christensen, E.R., 1982. A model for radionuclides in sediments influenced by mixing and compaction. J. Geophys. Res. 87 (C1), 566–572. https://doi.org/10.1029/JC087iC01p00566.

Clem, K.R., Renwick, J.A., McGregor, J., 2017. Large-scale forcing of the Amundsen Sea Low and its influence on sea ice and West Antarctic temperature. J. Clim. 30, 8405–8424. https://doi.org/10.1175/JCLI-D-16-0891.1.

Core Team, R., 2017. R: A Language and Environment for Statistical Computing. https://www.R-project.org/.

Crosta, X., Sturm, A., Armand, L., Pichon, J.-J., 2004. Late Quaternary Sea ice history in the Indian sector of the Southern Ocean as recorded by diatom assemblages. Mar. Micropaleontol. 50 (3–4), 209–223. https://doi.org/10.1016/S0377-7808398(03)00072-0.

De Deckker, P., Norman, M., Goodwin, I., Wain, A., Gingele, F., 2010. Lead isotopic evidence for an Australian source of aeolian dust to Antarctica at times over the last 170,000 years. Palaeogeogr. Palaeoclimatol. Palaeoecol. 285, 205223. https://doi.org/10.1016/j.palaeo.2009.11.013.

DeConto, R.M., Pollard, D., 2016. Contribution of Antarctica to past and future sea-level rise. Nature 531, 591–597. https://doi.org/10.1038/nature17145.

Delmont, T.O., Hammar, K.M., Ducklow, H.W., Yager, P.L., Post, A.F., 2014. *Phaeocystis antarctica* blooms strongly influence bacterial community structures in the Amundsen Sea polynya. Front. Microbiol. 5, 646. https://doi.org/10.3389/fmicb.2014.00646.

DeMaster, D.J., Cochran, J.K., 1982. Particle mixing rates in deep-sea sediments determined from excess ^{210}Pb and ^{32}Si profiles. Earth Planet. Sci. Lett. 61, 257–271.

Diaz, R.J., 2001. Overview of hypoxia around the world. J. Environ. Qual. 30, 275–281. https://doi.org/10.2134/jeq2001.302275x.

Din, Z., 1992. Use of aluminum to normalize heavy-metal data from estuarine and coastal sediments of Straits of Melaka. Mar. Pollut. Bull. 24, 484–491. https://doi.org/10.1016/0025-326X(92)90472-I.

Dixon, D.A., Mayewski, P.A., Goodwin, I.D., Marshall, G.J., Freeman, R., Maasch, K.A., Sneed, S.B., 2011. An ice-core proxy for northerly air mass incursions into West Antarctica. Int. J. Climatol. 32, 1455–1465. https://doi.org/10.1002/joc.2371.

Domack, E.W., Ishman, S.E., Stein, A.B., Jull, A.J.T., 1995. Late Holocene advance of the Müller Ice Shelf, Antarctic Peninsula: sedimentological, geochemical and palaeontological evidence. Antarct. Sci. 7, 159–170. https://doi.org/10.1017/S0954102095000228.

Dotto, T.S., Naveira Garabato, A.C., Wåhlin, A.K., Bacon, S., Holland, P.R., Kimura, S., Tsamados, M., Herraiz-Borreguero, L., Kalén, O., Jenkins, A., 2020. Control of the oceanic heat content of the Getz-Dotson Trough, Antarctica, by the Amundsen Sea Low. J. Geophys. Res. Oceans 125, e2020JC016113. https://doi.org/10.1029/2020JC016113.

Duprat, L.P.A.M., Bigg, G.R., Wilton, D.J., 2016. Giant icebergs significantly enhance the marine productivity of the Southern Ocean. Nat. Geosci. 9, 219–221. https://doi.org/10.1038/ngeo2633.

Dutrieux, P., Rydt, J.D., Jenkins, A., Holland, P.R., Ha, H.K., Lee, S.H., Steig, E.J., Ding, Q., Abrahamsen, E.P., Schröder, M., 2014. Strong sensitivity of Pine Island ice-shelf melting to climatic variability. Science 343, 174–178. https://doi.org/10.1126/science.1244341.

Emile-Geay, J., Cobb, K.M., Mann, M.E., Wittenberg, A.T., 2013. Estimating central equatorial Pacific SST variability over the past millennium part II: Reconstructions and implications. J. Clim. 26 (7), 2329–2352. https://doi.org/10.1175/JCLI-D-11-00511.1.

Esper, O., Gersonde, R., 2014a. Quaternary surface water temperature estimations: new diatom transfer functions for the Southern Ocean. Palaeogeogr. Palaeoclimatol. Palaeoecol. 414, 1–19. https://doi.org/10.1016/J.PALAEO.2014.08.008.

Esper, O., Gersonde, R., 2014b. New tools for the reconstruction of Pleistocene Antarctic Sea ice. Palaeogeogr. Palaeoclimatol. Palaeoecol. 399, 260–283. https://doi.org/10.1016/J.PALAEO.2014.01.019.

Esper, O., Gersonde, R., Kadagies, N., 2010. Diatom distribution in southeastern Pacific surface sediments and their relationship to modern environmental variables. Palaeogeogr. Palaeoclimatol. Palaeoecol. 287 (1–4), 1–27. https://doi.org/10.1016/j.palaeo.2009.12.006.

Falkowski, P.G., Greene, M., Geider, R.J., 1992. Physiological limitations on phytoplankton productivity in the ocean. Oceanography 5, 84–91. https://doi.org/10.5670/oceanog.1992.14.

Favier, L., Durand, G., Cornford, S.L., Gudmundsson, G.H., Gagliardini, O., Gillet-Chaulet, F., Zwinger, T., Payne, A.J., Le Brocq, A.M., 2014. Retreat of Pine Island Glacier controlled by marine ice-sheet instability. Nat. Clim. Chang. 4 (2), 117–121. https://doi.org/10.1038/NCLIMATE2094.

Friedrich, J., Janssen, F., Aleynik, D., Bange, H.W., Boltacheva, N., Çagatay, M.N., Dale, A.W., Etiope, G., Erdem, Z., Geraga, M., Gilli, A., Gomoiu, M.T., Hall, P.O.J., Hansson, D., He, Y., Holtappels, M., Kirf, M.K., Kononets, M., Konovalov, S., Lichtschlag, A., Livingstone, D.M., Marinaro, G., Mazlumyan, S., Naeher, S., North, R.P., Papatheodorou, G., Pfannkuche, O., Prien, R., Rehder, G., Schubert, C.J., Soltwedel, T., Sommer, S., Stahl, H., Stanev, E.V., Teaca, A., Tengberg, A., Waldmann, C., Wehrli, B., Wenzhöfer, F., 2014. Investigating hypoxia in aquatic environments: diverse approaches to addressing a complex phenomenon. Biogeosciences 11, 1215–1259. https://doi.org/10.5194/bg-11-1215-2014.

Gerringa, L.J.A., Alderkamp, A.-C., Laan, P., Thuróczy, C.-E., De Baar, H.J.W., Mills, M. M., van Dijken, G.L., van Haren, H., Arrigo, K.R., 2012. Iron from melting glaciers fuels the phytoplankton blooms in Amundsen Sea (Southern Ocean): iron biogeochemistry. Deep-Sea Res. II 71-76, 16–31. https://doi.org/10.1016/j.dsr2.2012.03.007.

Gersonde, R., Zielinski, U., 2000. The reconstruction of late quaternary Antarctic sea-ice distribution — the use of diatoms as a proxy for sea-ice. Palaeogeogr. Palaeoclimatol. Palaeoecol. 162, 263–286. https://doi.org/10.1016/S0031-0182(00)00131-0.

Gillett, N.P., Fyfe, J.C., 2013. Annular mode changes in the CMIP5 simulations. Geophys. Res. Lett. 40, 1189–1193.

Gloersen, P., Campbell, W.J., Cavalieri, D.J., Comiso, J.C., Parkinson, C.L., Zwally, H.J., 1993. Arctic and antarctic sea ice, 1978-1987. Ann. Glaciol. 17, 149–154.

Grove, J.M., 2004. Little Ice Ages: Ancient and Modern. Routledge, London and New York, 718 p.

Hillenbrand, C.-D., Smith, J.A., Hodell, D.A., Greaves, M., Poole, C.R., Kender, S., Williams, M., Andersen, T.J., Jernas, P.E., Elderfield, H., Klages, J.P., Roberts, S.J., Gohl, K., Larter, R.D., Kuhn, G., 2017. West Antarctic ice sheet retreat driven by Holocene warm water incursions. Nature 547, 43–48. https://doi.org/10.1038/nature22995.

Horne, R.A., 1969. Marine Chemistry the Structure of Water and the Chemistry Hydrosphere. Wiley, New York, 568 p.

Hosking, J.S., Orr, A., Marshall, G.J., Turner, J., Phillips, T., 2013. The influence of the Amundsen-Bellingshausen seas low on the climate of West Antarctica and its representation in coupled climate model simulations. J. Clim. 26, 6633–6648.

Hutson, W.H., 1980. The Agulhas current during the late Pleistocene: analysis of modern faunal analogs. Science 207 (4426), 64–66. https://doi.org/10.1126/science.207.4426.64.

Imbrie, J., Kipp, N.G., 1971. A new micropaleontological method for quantitative paleoclimatology: application to a late Pleistocene Caribbean core. In: Turekian, K.K. (Ed.), The Late Cenozoic Glacial Ages. Yale University Press, New Haven, Connecticut, pp. 71–181.

Jankowska, E., Michel, L.N., Zaborska, A., Włodarska-Kowalczuk, M., 2016. Sediment carbon sink in low-density temperate eelgrass meadows (Baltic Sea). J. Geophys. Res. Biogeosci. 121, 2918–2934. https://doi.org/10.1002/2016JG003424.

Jenkins, A., Shoosmith, D., Dutrieux, P., Jacobs, S., Kim, T.W., Lee, S.H., Ha, H.K., Stammerjohn, S., 2018. West Antarctic Ice Sheet retreat in the Amundsen Sea driven by decadal oceanic variability. Nat. Geosci. 11 (10), 733–738. https://doi.org/10.1038/s41561-018-0207-4.

Kim, T.W., 2020. Ocean-to-Ice interactions in Amundsen Sea: ice Shelf melting and its impact on ocean processes. Research Report, Korea Polar Research Institute. P.142. http://library.kopri.re.kr/search/detail/CATTOT000000054469.

Kim, M., Hwang, J., Lee, S.H., Kim, H.J., Kim, D., Yang, E.J., Lee, S.H., 2016. Sedimentation of particulate organic carbon on the Amundsen Shelf, Antarctica. Deep-Sea Res. II 123, 135–144. https://doi.org/10.1016/j.dsr2.2015.07.018.

Kim, I., Hahm, D., Park, K., Lee, Y., Choi, J.-O., Zhang, M., Chen, L., Kim, H.-C., Lee, S.H., 2017. Characteristics of the horizontal and vertical distributions of dimethyl sulfide throughout the Amundsen Sea Polynya. Sci. Total Environ. 584-585, 154–163. https://doi.org/10.1016/j.scitotenv.2017.01.165.

Kimura, S., Jenkins, A., Regan, H., Holland, P.R., Assmann, K.M., Whitt, D.B., Van Wessem, M., van de Berg, W.J., Reijmer, C.H., Dutrieux, P., 2017. Oceanographic controls on the variability of ice-shelf basal melting and circulation of glacial meltwater in the Amundsen Sea Embayment, Antarctica. J. Geophys. Res. Oceans 122, 10,131–10,155. https://doi.org/10.1002/2017JC012926.

Kirshner, A., Anderson, J.B., Jakobsson, M., O'Regan, M., Majewski, W., Nitsche, F., 2012. Post-LGM deglaciation in Pine island Bay, West Antarctica. Quat. Sci. Rev. 38, 11–26.

Klages, J.P., Kuhn, G., Hillenbrand, C.-D., Smith, J.A., Graham, A.G.C., Nitsche, F.O., Frederichs, T., Jernas, P.E., Gohl, K., Wacker, L., 2017. Limited grounding-line advance onto the West Antarctic continental shelf in the easternmost Amundsen Sea Embayment during the last glacial period. PLoS One 12 (7), e0181593. https://doi.org/10.1371/journal.pone.0181593.

Koch, J., Kilian, R., 2005. 'Little Ice Age' glacier fluctuations, Gran Campo Nevado, southernmost Chile. The Holocene 15, 20–28. https://doi.org/10.1191/0959683605hl780rp.

Koffman, B.G., Kreutz, K.J., Breton, D.J., Kane, E.J., Winski, D.A., Birkel, S.D., Kurbatov, A.V., Handley, M.J., 2014. Centennial-scale variability of the Southern Hemisphere westerly wind belt in the eastern Pacific over the past two millennia. Clim. Past 10, 1125–1144. https://doi.org/10.5194/cp-10-1125-2014.

Krause, G.H., Weis, E., 1991. Chlorophyll fluorescence and photosynthesis: the basics. Annu. Rev. Plant Physiol. Plant Mol. Biol. 42, 313–349. https://doi.org/10.1146/annurev.pp.42.060191.001525.

Lamping, N., Müller, J., Esper, O., Hillenbrand, C.-D., Smith, J.A., Kuhn, G., 2020. Highly branched isoprenoids reveal onset of deglaciation followed by dynamic sea-ice conditions in the western Amundsen Sea, Antarctica. Quat. Sci. Rev. 228, 106103. https://doi.org/10.1016/j.quascirev.2019.106103.

Langone, L., Frignani, M., Labbrozzi, L., Ravaioli, M., 1998. Present-day biosiliceous sedimentation in the NW Ross Sea (Antartica). J. Mar. Syst. 17, 459–470.

Larter, R.D., Anderson, J.B., Graham, A.G.C., Gohl, K., Hillenbrand, C.-D., Jakobsson, M., Johnson, J.S., Kuhn, G., Nitsche, F.O., Smith, J.A., Witus, A.E., Bentley, M.J., Dowdeswell, J.A., Ehrmann, W., Klages, J.P., Lindow, J., ÓCofaigh, C., Spiegel, C., 2014. Reconstruction of changes in the Amundsen Sea and Bellingshausen Sea sector of the West Antarctic Ice Sheet since the Last Glacial Maximum. Quat. Sci. Rev. 100, 55–86. https://doi.org/10.1016/j.quascirev.2013.10.016.

Lee, Y., Yang, E.J., Park, J., Jung, J., Kim, T.W., Lee, S.H., 2016. Physical-biological coupling in the Amundsen Sea, Antarctica: influence of physical factors on phytoplankton community structure and biomass. Deep-Sea Res. I 117, 51–60. https://doi.org/10.1016/j.dsr.2016.10.001.

Li, F., Ginoux, P., Ramaswamy, V., 2008. Distribution, transport, and deposition of mineral dust in the Southern Ocean and Antarctica: contribution of major sources. J. Geophys. Res. 113, D10207 https://doi.org/10.1029/2007jd009190.

Li, J., Xie, S.P., Cook, E., Morales, M.S., Christie, D.A., Johnson, N.C., Chen, F., D'Arrigo, R., Fowler, A.M., Gou, X., Fang, K., 2013. El Niño modulations over the past seven centuries. Nat. Clim. Chang. 3, 822–826. https://doi.org/10.1038/nclimate.

Lilien, D.A., Joughin, I., Smith, B., Shean, D.E., 2018. Changes in flow of Crosson and Dotson ice shelves, West Antarctica, in response to elevated melt. Cryosphere 12, 1415–1431. https://doi.org/10.5194/tc-12-1415-2018.

Lim, D.I., Xu, Z., Choi, J.Y., Kim, S.Y., Kim, E.H., Kang, S., Jung, H.S., 2011. Paleoceanographic changes in the Ulleung Basin, East (Japan) Sea, during the last 20,000 years: evidence from variations in element composition of core sediments. Prog. Oceanogr. 88, 101–115. https://doi.org/10.1016/j.pocean.2010.12.016.

Liu, J., Curry, J.A., Martinson, D.G., 2004. Interpretation of recent Antarctic Sea ice variability. Geophys. Res. Lett. 31, L02205 https://doi.org/10.1029/2003GL018732.

Mahowald, N.M., Kloster, S., Engelstaedter, S., Moore, J.K., Mukhopadhyay, S., McConell, J.R., Albani, S., Doney, S.C., Bhattacharya, A., Curran, M.A.J., Flanner, M. G., Hoffmann, F.M., Lawrence, D.M., Lindsay, K., Mayewski, P.A., Neff, J., Rothenberg, D., Thomas, E., Thornton, P.E., Zender, C.S., 2010. Observed 20th century desert dust variability: impact on climate and biogeochemistry. Atmos. Chem. Phys. 10, 10875–10893. https://doi.org/10.5194/acp-10-10875-2010.

Mankoff, K.D., Jacobs, S.S., Tulaczyk, S.M., Stammerjohn, S.E., 2012. The role of Pine Island Glacier ice shelf basal channels in deep-water upwelling, polynyas and ocean circulation in Pine Island Bay, Antarctica. Ann. Glaciol. 53 (60), 123–128. https://doi.org/10.3189/2012AoG60A062.

Maqueda, M.M., Willmott, A.J., Biggs, N.R.T., 2004. Polynya dynamics: a review of observations and modeling. Rev. Geophys. 42, RG1004 https://doi.org/10.1029/2002RG000116.

Marshall, G.J., 2003. Trends in the Southern annular mode from observations and reanalyses. J. Clim. 16, 4134–4143. https://doi.org/10.1175/1520-0442(2003)016%3C4134:TITSAM%3E2.0.CO;2.

Masqué, P., Isla, E., Sanchez-Cabeza, J.A., Palanques, A., Bruach, J.M., Puig, P., Guillén, J., 2002. Sediment accumulation rates and carbon fluxes to bottom sediments at the Western Bransfield Strait (Antarctica). Deep-Sea Res. II 49, 921–933.

Masson-Delmotte, V., Schulz, M., Abe-Ouchi, A., Beer, J., Ganopolski, A., Gonzalez Rouco, J.F., Jansen, E., Lambeck, K., Luterbacher, J., Naish, T., Osborn, T., Otto-Bliesner, B., Quinn, T., Ramesh, R., Rojas, M., Shao, X., Timmermann, A., 2013. In: Stocker, T.F., Qin, D., Plattner, G.-K., Tignor, M.M.B., Allen, S.K., Boschung, J., Midgley, P.M. (Eds.), Climate Change 2013: the Physical Science Basis: Contribution of Working Group I to the Fifth Assessment Report of the Intergovernmental Panel on Climate Change. Cambridge University Press, pp. 383–464.

McKinzey, K.M., Lawson, W., Kelly, D., Hubbard, A., 2004. A revised Little Ice Age chronology of the Franz Josef Glacier, Westland, New Zealand. J. R. Soc. N. Z. 34, 381–394. https://doi.org/10.1080/03014223.2004.9517774.

Milillo, P., Rignot, E., Rizzoli, P., Scheuchl, B., Mouginot, J., Bueso-Bello, J., Prats-Iraola, P., 2019. Heterogeneous retreat and ice melt of Thwaites Glacier, West Antarctica. Sci. Adv. 5 (1), eaau3433. https://doi.org/10.1126/sciadv.aau3433.

Moline, M., Claustre, H., Frazer, T.K., Schofield, O., Vernet, M., 2004. Alteration of the food web along the Antarctic Peninsula in response to a regional warming trend. Glob. Chang. Biol. 10, 1973–1980.

Morford, J.L., Emerson, S., 1999. The geochemistry of redox sensitive trace metals in sediments. Geochim. Cosmochim. Acta 63, 1735–1750. https://doi.org/10.1016/S0016-7037(99)00126-X.

Mortlock, R.A., Froelich, P.N., 1989. A simple and reliable method for the rapid determination of biogenic opal in pelagic sediments. Deep-Sea Res. 36 (9), 1415–1426.

Mouginot, J., Rignot, E., Scheuchl, B., 2014. Sustained increase in ice discharge from the Amundsen Sea Embayment, West Antarctica, from 1973 to 2013. Geophys. Res. Lett. 41, 1576–1584. https://doi.org/10.1002/2013GL059069.

Moussa, A.A., 1983. Trace elements in recent sediments of the Nile Delta continental shelf: their accumulation and significance. 6th Workshop on pollution of the Mediterranean (Cannes, 2-4 December 1982), pp. 401–404.

Müller, P.J., Schneider, R., 1993. An automated leaching method for the determination of opal in sediments and particulate matter. Deep-Sea Res. 40, 425–444.

Muñoz, P., Dezileau, L., Lange, C., Cardenas, L., Sellanes, J., Salamanca, M.A., Maldonado, A., 2012. Evaluation of sediment trace metal records as paleoproductivity and paleoxygenation proxies in the upwelling center off Concepción, Chile (36°S). Prog. Oceanogr. 92-95, 66–80. https://doi.org/10.1016/j.pocean.2011.07.010.

Naidu, A.S., Blanchand, A., Kellet, J.J., Goering, J.J., Hameedi, M.J., Caskaran, M., 1997. Heavy metals in Chukchi Sea sediments as compared to selected Circum-Arctic shelves. Mar. Pollut. Bull. 35, 260–269.

Nakayama, Y., Menemenlis, D., Zhang, H., Schodlok, M., Rignot, E., 2018. Origin of Circumpolar Deep Water intruding onto the Amundsen and Bellingshausen Sea continental shelves. Nat. Commun. 9, 3403. https://doi.org/10.1038/s41467-018-05813-1.

Nittrouer, C.A., Sternberg, R.W., Carpenter, R., Bennett, J.T., 1970. The use of Pb-210 geochronology as a sedimentological tool: application to the Washington continental shelf. Mar. Geol. 31 (3–4), 297–316.

Oksanen, J., Blanchet, F.G., Kindt, R., Legendre, P., Minchin, P.R., O'Hara, R.B., Simpson, G.L., Solymos, P., Stevens, M.H.H., Wagner, H., 2012. Vegan: Community Ecology Package (R Package Version 2.0–3).
Olbers, D., Gouretski, V.V., Seiß, G., Schröter, J., 1992. Hydrographic Atlas of the Southern Ocean. Alfred Wegener Institute for Polar and Marine Research. Bremerhaven, Germany & Arctic and Antarctic Research Institute, St. Petersburg, Russia, 17pp.
Paasche, Ø., Bakke, J., 2010. Defining the Little Ice Age. Clim. Past Discuss. 6, 2159–2175. https://doi.org/10.5194/cpd-6-2159-2010.
Paolo, F.S., Fricker, H.A., Padman, L., 2015. Volume loss from Antarctic ice shelves is accelerating. Science 348, 327–331. https://doi.org/10.1126/science.aaa0940.
Peloquin, J.A., Smith Jr., W.O., 2007. Phytoplankton blooms in the Ross Sea, Antarctica: interannual variability in magnitude, temporal patterns, and composition. J. Geophys. Res. 112, C08013 https://doi.org/10.1029/2006JC003816.
Presley, B.J., 1997. A review of arctic trace metal data with implications for biological effects. Mar. Pollut. Bull. 35, 226–234.
Pritchard, H.D., Ligtenberg, S.R.M., Fricker, H.A., Vaughan, D.G., van den Broeke, M.R., Padman, L., 2012. Antarctic ice-sheet loss driven by basal melting of ice shelves. Nature 484 (7395), 502–505. https://doi.org/10.1038/nature10968.
Rabalais, N.N., Díaz, R.J., Levin, L.A., Turner, R.E., Gilbert, D., Zhang, J., 2010. Dynamics and distribution of natural and human-caused hypoxia. Biogeosciences 7, 585–619. https://doi.org/10.5194/bg-7-585-2010.
Raiswell, R., Benning, L.G., Tranter, M., Tulaczyk, S., 2008. Bioavailable iron in the Southern Ocean: the significance of the iceberg conveyor belt. Geochem. Trans. 9, 7. https://doi.org/10.1186/1467-4866-9-7.
Raiswell, R., Hawkings, J.R., Benning, L.G., Baker, A.R., Death, R., Albani, S., Mahowald, N., Krom, M.D., Poulton, S.W., Wadham, J., Tranter, M., 2016. Potentially bioavailable iron delivery by iceberg-hosted sediments and atmospheric dust to the polar oceans. Biogeosciences 13, 3887–3900. https://doi.org/10.5194/bg-13-3887-2016.
Reynolds, R.W., Rayner, N.A., Smith, T.M., Stokes, D.C., Wang, W., 2002. An improved in situ and satellite SST analysis for climate. J. Clim. 15 (13), 1609–1625 doi:10.1175/1520-0442(2002)015<1609:AIISAS>2.0.CO;2.
Reynolds, R.W., Smith, T.M., Liu, C., Chelton, D.B., Casey, K.S., Schlax, M.G., 2007. Daily high-resolution-blended analyses for sea surface temperature. J. Clim. 20 (22), 5473–5496. https://doi.org/10.1175/2007JCLI1824.1.
Rignot, E., Jacobs, S., Mouginot, J., Scheuchl, B., 2013. Ice-shelf melting around Antarctica. Science 341, 266–270. https://doi.org/10.1126/science.1235798.
Rignot, E., Mouginot, J., Morlighem, M., Seroussi, H., Scheuchl, B., 2014. Widespread, rapid grounding line retreat of Pine Island, Thwaites, Smith, and Kohler glaciers, West Antarctica, from 1992 to 2011. Geophys. Res. Lett. 41, 3502–3509. https://doi.org/10.1002/2014GL060140.
Robbins, J., Edgington, D., 1975. Determination of recent sedimentation rates in Lake Michigan using Pb-210 and Cs-137. Geochim. Cosmochim. Acta 39 (3), 285–304.
Robbins, J.A., Herche, L.R., 1993. Models and uncertainty in ^{210}Pb dating of sediments. Verhandlungen des Internationalen Verein Limnologie 25, 217–222.
Rose, J.M., Feng, Y., DiTullio, G.R., Dunbar, R.B., Hare, C.E., Lee, P.A., Lohan, M., Long, M., Smith Jr., W.O., Sohst, B., Tozzi, S., Zhang, Y., Hutchins, D.A., 2009. Synergistic effects of iron and temperature on Antarctic phytoplankton and microzooplankton assemblages. Biogeosciences 6, 3131–3147.
Sanders, C.J., Smoak, J.M., Sanders, L.M., Waters, M.N., Patchineelam, S.R., Ketterer, M. E., 2010. Intertidal mangrove mudflat 240+239Pu signatures, confirming a ^{210}Pb geochronology on the southeastern coast of Brazil. J. Radioanal. Nucl. Chem. 283, 593–596. https://doi.org/10.1007/s10967-009-0418-7.
Schofield, O., Miles, T., Alderkamp, A.-C., Lee, S.H., Haskins, C., Rogalsky, E., Sipler, R., Sherrell, R.M., Yager, P.L., 2015. *In situ* phytoplankton distributions in the Amundsen Sea Polynya measured by autonomous gliders. Elementa: Sci. Anthropocene 3. https://doi.org/10.12952/journal.elementa.000073, 000073.
Schrader, H., Gersonde, S., 1978. Diatoms and silicoflagellates. In: Zachariasse, W.J., et al. (Eds.), Microplaeontological counting methods and techniques - an exercise on an eight metres section of the lower Pliocene of Capo Rossello. Sicily. Utrecht Micropaleontological Bulletins, 17, pp. 129–176.
Schropp, S.J., Lewis, F.G., Windom, H.L., Ryan, J.D., Calder, F.D., Burney, L.C., 1990. Interpretation of metal concentrations in estuarine sediments of Florida using aluminum as a reference element. Estuaries 13 (3), 227–235.
Schwarz, J.N., Schodlok, M.P., 2009. Impact of drifting icebergs on surface phytoplankton biomass in the Southern Ocean: Ocean colour remote sensing and in situ iceberg tracking. Deep-Sea Res. Part I: Oceanogr. Res. Pap. 56, 1727–1741.
Sedwick, P.N., Garcia, N.S., Riseman, S.F., Marsay, C.M., DiTullio, G.R., 2007. Evidence for high iron requirements of colonial Phaeocystis Antarctica at low irradiance. Biogeochemistry 83, 83–97.
Serrano, O., Ruhon, R., Lavery, P.S., Kendrick, G.A., Hickey, S., Masqué, P., Arias-Ortiz, A., Steven, A., Duarte, C.M., 2016. Impact of mooring activities on carbon stocks in seagrass meadows. Sci. Rep. 6, 23193. https://doi.org/10.1038/srep23193.
Sherrell, R.M., Lagerstrom, M.E., Forsch, K.O., Stammerjohn, S.E., Yager, P.L., 2015. Dynamics of dissolved iron and other bioactive trace metals (Mn, Ni, Cu, Zn) in the Amundsen Sea Polynya, Antarctica. Elementa: Sci. Anthropocene 3, 71. https://doi.org/10.12952/journal.elementa.000071.
Simpson, G.L., Oksanen, J., 2012. analogue: Analogue and Weighted Averaging Methods For Palaeoecology. Version 0.9–5. http://analogue.r-forge.r-project.org/.
Smith Jr., W.O., Comiso, J.C., 2008. The influence of sea ice on primary production in the Southern Ocean: a satellite perspective. J. Geophys. Res. 113, C05S93 https://doi.org/10.1029/2007JC004251.
Soetaert, K., Herman, P.M.J., Middelburg, J.J., 1996. A model of early diagenetic processes from the shelf to abyssal depths. Geochim. Cosmochim. Acta 60 (6), 1019–1040.
Stammerjohn, S.E., Martinson, D.G., Smith, R.C., Yuan, X., Rind, D., 2008. Trends in Antarctic annual sea ice retreat and advance and their relation to El Niño–Southern Oscillation and Southern Annular Mode variability. J. Geophys. Res. 113, C03S90 https://doi.org/10.1029/2007JC004269.
Stammerjohn, S.E., Maksym, T., Massom, R.A., Lowry, K.E., Arrigo, K.R., Yuan, X., Raphael, M., Randall-Goodwin, E., Sherrell, R.M., Yager, P.L., 2015. Seasonal Sea ice changes in the Amundsen Sea, Antarctica, over the period of 1979–2014. Elementa: Sci. Anthropocene 3. https://doi.org/10.12952/journal.elementa.000055, 000055.
St-Laurent, P., Yager, P.L., Sherrell, R.M., Stammerjohn, S.E., Dinniman, M.S., 2017. Pathways and supply of dissolved iron in the Amundsen Sea (Antarctica). J. Geophys. Res. 122, 7135–7162. https://doi.org/10.1002/2017JC013162.
Strelin, J., Casassa, G., Rosqvist, G., Holmund, P., 2008. Holocene glaciations in the Ema Glacier Valley, Monte Sarmiento Massif, Tierra del Fuego. Palaeogeogr. Palaeoclimatol. Palaeoecol. 260, 299–314. https://doi.org/10.1016/j.palaeo.2007.12.002.
Sutterley, T.C., Velicogna, I., Rignot, E., Mouginot, J., Flament, T., van den Broeke, M.R., van Wessem, J.M., Reijmer, C.H., 2014. Mass loss of the Amundsen Sea Embayment of West Antarctica from four independent techniques. Geophys. Res. Lett. 41, 8421–8428. https://doi.org/10.1002/2014GL061940.
Taylor, F., Whitehead, J., Domack, E., 2001. Holocene paleoclimate change in the Antarctic Peninsula: evidence from the diatom, sedimentary and geochemical record. Mar. Micropaleontol. 41 (1–2), 25–43. https://doi.org/10.1016/S0377-8398(00)00049-9.
Taylor, M.H., Losch, M., Bracher, A., 2013. On the drivers of phytoplankton blooms in the Antarctic marginal ice zone: a modeling approach. J. Geophys. Res. Oceans 118, 63–75. https://doi.org/10.1029/2012JC008418.
Thoma, M., Jenkins, A., Holland, D., Jacobs, S., 2008. Modelling circumpolar deep water intrusions on the Amundsen Sea continental shelf, Antarctica. Geophys. Res. Lett. 35, L18602 https://doi.org/10.1029/2008GL034939.
Thompson, D.W.J., Solomon, S., Kushner, P.J., England, M.H., Grise, K.M., Karoly, D.J., 2011. Signatures of the Antarctic ozone hole in Southern Hemisphere surface climate change. Nat. Geosci. 4, 741–749.
Tortell, P.D., Long, M.C., Payne, C.P., Alderkamp, A.-C., Arrigo, K.R., 2012. Spatial distribution of pCO2, DO2/Ar and dimethylsulfide (DMS) in Polynya waters and the sea ice zone of the Amundsen Sea, Antarctica. Deep-Sea Res. II 71-76, 77–93. https://doi.org/10.1016/j.dsr2.2012.03.010.
Turekian, K., Cochran, K., Benninger, L., Aller, R., 1980. The sources and sinks of nuclides in LongIsland Sound. Adv. Geophys. 22, 129–163.
Turner, J., Orr, A., Gudmundsson, G.H., Jenkins, A., Bingham, R.G., Hillenbrand, C.-D., Bracegirdle, T.J., 2017. Atmosphere-ocean-ice interactions in the Amundsen Sea Embayment, West Antarctica. Rev. Geophys. 55, 235–276. https://doi.org/10.1002/2016RG000532.
Vorrath, M.-E., Müller, J., Rebolledo, L., Cárdenas, P., Shi, X., Esper, O., Opel, T., Geibert, W., Muñoz, P., Haas, C., Kuhn, G., Lange, C.B., Lohmann, G., Mollenhauer, G., 2020. Sea ice dynamics in the Bransfield Strait, Antarctic Peninsula, during the past 240 years: a multi-proxy intercomparison study. Clim. Past 16, 2459–2483. https://doi.org/10.5194/cp-16-2459-2020.
Wallace, R.B., Baumann, H., Grear, J.S., Aller, R.C., Gobler, C.J., 2014. Coastal Ocean acidification: the other eutrophication problem. Estuar. Coast. Shelf Sci. 148, 1–13. https://doi.org/10.1016/j.ecss.2014.05.027.
Wang, S., Bailey, D., Lindsay, K., Moore, J.K., Holland, M., 2014. Impact of sea ice on the marine iron cycle and phytoplankton productivity. Biogeosciences 11, 4713–4731. https://doi.org/10.5194/bg-11-4713-2014.
Winkler, S., 2009. First attempt to combine terrestrial cosmogenic nuclide (10Be) and Schmidt hammer relative-age dating: Strauchon Glacier, Southern Alps, New Zealand. Cent. Eur. J. Geosci. 1, 274–290.
Xiao, X., Fahl, K., Stein, R., 2013. Biomarker distributions in surface sediments from the Kara and Laptev seas (Arctic Ocean): indicators for organic-carbon sources and sea-ice coverage. Quat. Sci. Rev. 79, 40–52. https://doi.org/10.1016/j.quascirev.2012.11.028.
Xu, K., Fu, F.-X., Hutchins, D.A., 2014. Comparative responses of two dominant Antarctic phytoplankton taxa to interactions between ocean acidification, warming, irradiance, and iron availability. Limnol. Oceanogr. 59 (6), 1919–1931. https://doi.org/10.4319/lo.2014.59.6.1919.
Xu, G., Liu, J., Pei, S., Kong, X., Hu, G., Gao, M., 2015. Source identification of aluminum in surface sediments of the Yellow Sea off the Shandong Peninsula. Acta Oceanol. Sin. 34 (12), 147–153.
Yuan, X., 2004. ENSO-related impacts on Antarctic sea ice: a synthesis of phenomenon and mechanisms. Antarct. Sci. 16 (4), 415–425. https://doi.org/10.1017/S0954102004002238.
Yuan, X., Martinson, D.G., 2001. The Antarctic Dipole and its predictability. Geophys. Res. Lett. 28 (18), 3609–3612.
Zwally, H.J., Comiso, J.C., Parkinson, C.L., Cavalieri, D.J., Gloersen, P., 2002. Variability of Antarctic Sea ice 1979–1998. J. Geophys. Res. 107 (C5), 3041. https://doi.org/10.1029/2000JC000733.